RESEARCH ARTICLE

Control of oblique shock wave/boundary layer interactions using plasma actuators

N. Webb · C. Clifford · M. Samimy

Abstract Localized arc filament plasma actuators (LAFPAs) are used for shock wave/boundary layer interaction induced separation control in a Mach 2.3 flow. The boundary layer is fully turbulent with a Reynolds number based on the incompressible momentum thickness of 22,000 and shape factor of 1.37, and the impinging shock wave is generated by a 10° compression ramp. The LAFPAs are observed to have significant control authority over the interaction. The main effect is the displacement of the reflected shock and most of the interaction region upstream by approximately one boundary layer thickness (~ 5 mm). The initial goal of the control was to manipulate the low-frequency ($St \sim 0.03$) unsteadiness associated with the interaction region. A detailed investigation of the effect of actuator placement, frequency, and duty cycle on the control authority indicates the actuators' primary control mechanism is not the manipulation of low-frequency unsteadiness. Detailed measurements and analysis indicate that a modification to the boundary layer through heat addition by the actuators is the control mechanism, despite the extremely small power input of the actuators.

Abbreviation

f	Frequency
H	Upstream boundary layer shape factor, subscript "i" indicates incompressible: δ^*/θ
L_{int}	Interaction length (mm)
St	Strouhal number, normalized frequency: $f\,L_{int}/U_\infty$

St_F	Strouhal number at which the actuators were operated
U_∞	Upstream freestream velocity
X	Streamwise coordinate (Fig. 2)
X_o	Streamwise location of the projected primary shock inviscid impingement point
X^*	Normalized streamwise coordinate: $(X–X_o)/L_{int}$
X_a^*	Normalized streamwise location of the actuators
α	Compression ramp angle
δ	Upstream boundary layer thickness
δ^*	Upstream boundary layer displacement thickness, subscript "i" indicates incompressible
θ	Upstream boundary layer momentum thickness, subscript "i" indicates incompressible
ρ_∞	Upstream freestream density

1 Introduction

Shock wave/boundary layer interactions are ubiquitous in high-speed flows, occurring in locations from transonic wings, to axial turbines, to mixed-compression inlets. These interactions are generally detrimental due to the imposition of an adverse pressure gradient on the boundary layer. Due to the response of the low momentum regions of the boundary layer, this has the potential to significantly degrade the boundary layer and result in separation when the shock wave is strong. Depending on the application, these effects (especially the onset of separation and the associated increase in unsteadiness and aerodynamic blockage) can cause severe consequences and result in significant performance degradation of the system. For example, in supersonic mixed-compression inlets, the boundary layer degradation can cause significant distortion,

N. Webb · C. Clifford · M. Samimy (✉)
Gas Dynamics and Turbulence Laboratory, Aeronautical and Astronautical Research Laboratories, The Ohio State University, 2300 West Case Road, Columbus, OH 43235, USA
e-mail: samimy.1@osu.edu

especially in the region of the subsonic diffuser. This can have significant effects on the operation of the compressor and the engine. Additionally, in the event of separation, the added aerodynamic blockage can choke the inlet triggering unstart and a loss of engine thrust. Boundary layer bleed has been the traditional control method: utilizing scoops, slots, and holes to remove low momentum boundary layer fluid and avoid severe shock wave/boundary layer interactions (SWBLIs) altogether (Syberg and Koncsek 1976). Boundary layer bleed also provides a variety of other benefits including inlet mass capture and engine demand balancing (Baruzzini 2012). In spite of its multiple benefits, bleed has inherent performance detriments that make minimization or elimination of bleed desirable.

To this end, the research community has been investigating a variety of separation control techniques for SWBLIs. Both passive and active techniques are being explored. One of the most prominent passive techniques is the use of vortex generators. These have been explored in a variety of shapes and sizes from large scale (height $\sim \delta$) (Shahneh and Motallebi 2009) to so-called micro-vortex generators: micro-vanes (Anderson et al. 2006), ramps (Babinsky et al. 2009; Lee et al. 2010), hybrid geometries (Lee et al. 2010), and other configurations. These studies seek to improve the boundary layer response to the shock-imposed pressure gradient by using streamwise vorticity to enhance mixing, thereby increasing momentum in the near-wall region. Vortex generator research also focuses on minimizing the inherent drag associated with these devices. Three-dimensional bumps have also been explored for SWBLI control. Babinsky and Ogawa (2008) have investigated the bumps' ability to smear/spread the shock impingement of a normal SWBLI to ease the sharp pressure gradient imposed on the boundary layer. An additional benefit of the bumps is that spreading the shock structure decreases total pressure loss through the shock system. Another passive flow control technique is the use of meso-flaps designed to induce momentum exchange between the downstream and upstream boundary layer (Gefroh et al. 2002).

Passive control is attractive because it does not require energy input or (usually) moving parts. Thus, passive flow control techniques are commonly robust and require minimal maintenance. The drawback is that the control is usually only effective near design conditions. Moreover, the presence of geometric modifications at off-design conditions still generates parasitic drag (and perhaps worse effects) even when no benefit is present. Although boundary layer bleed is relatively flexible, this quality is far from typical among passive control techniques. Active flow control can often address this issue. Although it requires energy to function, and consequently imposes a parasitic drain on system resources, its nature allows it to adjust its

operation and consequently its power consumption. Researchers have examined active control methods for separation control in SWBLIs. Kalra et al. (2011) investigated the use of magnetohydrodynamic discharge actuators to add momentum to the near-wall flow, thereby delaying separation. Micro-jets (Solomon et al. 2010; Souverein and Debiève 2010) and zero-net-mass-flux pulsed-plasma jets (Narayanaswamy et al. 2012) have also been used to act as virtual/aerodynamic vortex generators. These generators could be turned on/off or altered based on flow conditions. Continuous or pulsed blowing has also been considered as a method of adding momentum to the boundary layer.

Active control can also function by introducing perturbations with tailored characteristics to exploit naturally occurring instabilities in the flow. Natural instabilities often manifest themselves through flow unsteadiness. Thus, unsteadiness in SWBLIs could indicate the presence of natural instabilities. Turbulence does result in minor unsteadiness in SWBLIs; however, the unsteadiness amplitude increases dramatically in separated interactions. A low-frequency unsteadiness has been observed in the region around the reflected shock (Touber and Sandham 2009; Dolling and Brusniak 1989; Dupont et al. 2006). This unsteadiness is broadband in nature, but centers about a frequency approximately two orders of magnitude lower than the freestream turbulence.

Researchers have long sought the source of this unsteadiness (Dolling 2001). Historically, there have been two primary theories: (1) that upstream fluctuations cause the low-frequency motion and (2) that downstream fluctuations are responsible. Researchers have examined the upstream boundary layer seeking to correlate the shock movement to various events such as bursting (Andreopoulos and Muck 1987) or streamwise elongated structures (Ganapathisubramani et al. 2009; Beresh et al. 2011). Those who support the downstream influence theory focus on the separation region. Pipponiau et al. (2009) proposed that periodic vortex shedding from the shear layer over the separation bubble causes a low-frequency expansion/contraction of the separation bubble, pushing the shock upstream and subsequently allowing it to relax downstream. This attributes the reflected shock unsteadiness to a Kelvin–Helmholtz type instability. Other theories propose an acoustic feedback loop in the separated region (Pirozzoli and Grasso 2006) or a global instability (Touber and Sandham 2009). Recent work by Narayanswamy (2010) seems to indicate that neither upstream nor downstream influences are solely responsible for the unsteadiness, rather a combination of the two. Upstream influence appears to be significant for incipiently or weakly separated interactions, while the downstream influences become dominant for stronger interactions. Analytical work by Touber and Sandham (2011) also seems to indicate that,

instead of being due to any particular perturbation, the unsteadiness is inherent to the coupled shock/boundary layer equations and is the natural manifestation of the perturbed system.

Localized arc filament plasma actuators (LAFPAs) were developed at The Ohio State University specifically for strong, high-frequency perturbation introduction (Utkin et al. 2007; Samimy et al. 2007a, b, 2010). This allows them to perturb a wide variety of flows. A significant amount of work has been done using LAFPAs as a noise mitigation and mixing enhancement control technique for high-speed, high-Reynolds number jets (Samimy et al. 2007a, b). The flexibility and dynamic nature of the LAFPAs also allows them to be used for feedback control (Sinha et al. 2010). The presence of natural unsteadiness in SWBLIs prompted an investigation of the LAFPAs' effectiveness for separation control in a SWBLI. Although, as discussed in Titchener et al. (2012), a single SWBLI may not be a realistic model of a mixed-compression inlet, which contains multiple SWBLIs and other types of adverse pressure gradients, a unit problem (single oblique impinging SWBLI, shown in Fig. 1) is a good starting point to verify the potential of LAFPAs for SWBLI separation control.

Previously, the LAFPAs' suitability for separation control in a SWBLI had been investigated and found to have potential (Caraballo 2009). A more in-depth work was begun by expanding the facility and its measurement capabilities (Webb et al. 2011). The present work continues to explore the LAFPAs' control authority in a SWBLI. Although the present work demonstrates that the results of the preliminary investigation were misinterpreted, it confirms the significant control authority of LAFPAs. This paper details modifications to the new test facility and a characterization of the baseline flow. Detailed velocity measurements of the flow using PIV for various forcing cases are presented and analyzed, and a potential control mechanism is discussed.
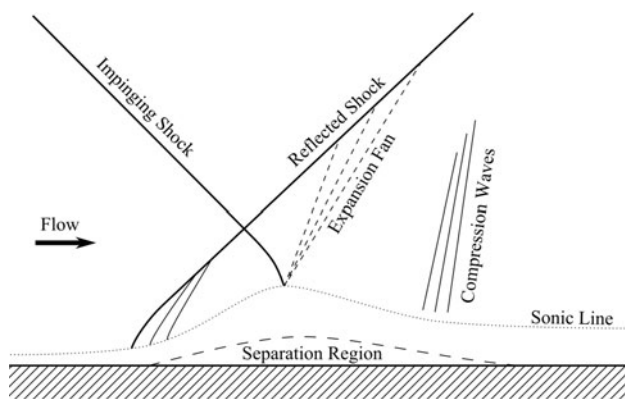

Fig. 1 Schematic of a strong SWBLI inducing separation

2 Experimental methodology

2.1 Physical arrangement

As previously mentioned, it was deemed appropriate to explore the separation control authority of the LAFPAs in a single oblique impinging SWBLI. The preliminary test facility was expanded (Webb et al. 2011) to that used for this work. It is a blow-down facility that uses compressed, dried air from large (~ 36 m^3) storage tanks. The stagnation pressure is controlled through a variable valve and electronic feedback control system. The test section is rectangular, 76.2 mm by 72.9 mm, the freestream Mach number is 2.33, and the stagnation temperature is measured in experiments and is approximately ambient. Optical access to the test section was provided by two nominally 76 mm high by 250 mm long fused quartz windows. A slit window in the test section ceiling allows for a centerline streamwise-vertical laser sheet. The facility described by Webb et al. (Webb et al. 2011) used a variable angle wedge to generate the primary impinging shock. A 10° compression ramp, which can be installed in three streamwise locations, was used to generate the primary shock in this work. This allows the streamwise location of the LAFPAs to be varied with respect to the SWBLI. Figure 2 is a schematic of the test section of the wind tunnel used in this work. It also defines the normalized streamwise coordinate (X^*) used to denote LAFPA placement and measurement locations.

Each LAFPA's physical configuration is two tungsten electrodes mounted with the tips flush to the tunnel floor. The electrodes are placed in a 1 mm wide by 0.5 mm deep groove in the tunnel floor. After air breakdown and formation of the plasma arc, this groove shields the arc and allows it to achieve a quasi-steady condition. The groove was shown to have a negligible effect on the control authority in jet experiments (Hahn et al. 2011). The tips of the electrodes are separated by 3.5 mm center-to-center, with a 5.2 mm separation between the nearest electrodes of two different actuators. Eight actuators are arranged in line across the span of the test section. The electrodes are configured such that the flow is normal to the line of electrodes/actuators. The inset of Fig. 2 shows a diagram of the LAFPAs' physical arrangement.

The actuators are operated by applying a high voltage across the two electrodes of each actuator. This induces breakdown in the air between the electrodes and a localized arc filament forms. The arc produces rapid localized heating generating a thermal (followed by a pressure) perturbation in the flow that can be used for flow control. The power supply used in this work (Utkin et al. 2007) allows the cycle of breakdown, quasi-steady arc formation, and shutdown to be repeated at a variable frequency up to

Fig. 2 Test section schematic with compression ramp model installed, inset: spanwise arrangement of the LAFPAs
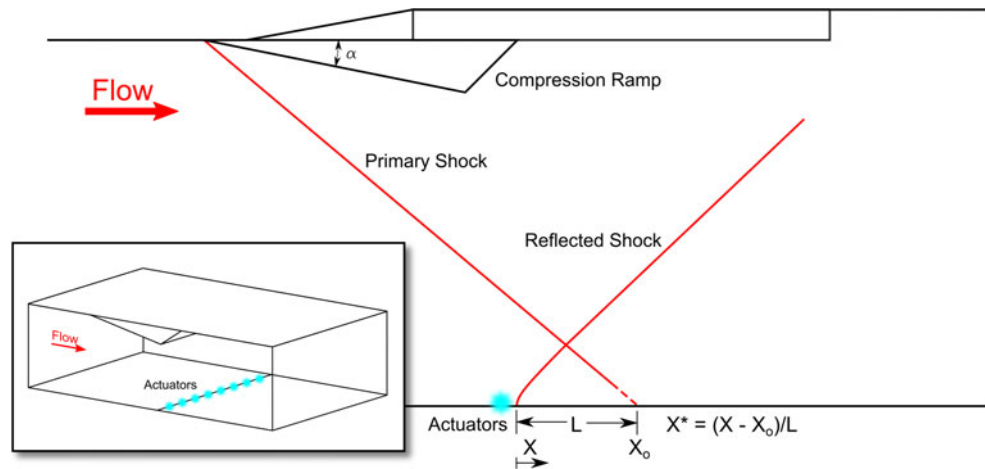
200 kHz. This work examines the effects of the LAFPAs on the flow when pulsed simultaneously and continuously. The physical configuration of the electrodes results in quasi-steady state arc formation, following the breakdown, with about a 400 V differential and 0.25 A current. Although the peak power release (immediately following breakdown) is much greater than the approximately time-averaged power of 100 W during quasi-steady arcing, for the relatively low frequencies (≤ 20 kHz) used in this study, the peak power release contributes a negligible amount to the time-averaged power. The time-averaged power input varies based on the duty cycle (percent of a period during which the actuators are arcing), for example, the power release with a 30 % duty cycle will be approximately 30 W per actuator. For the majority of this work, the duty cycle was 50 %, which means that the total power release was approximately 400 W for the 8 actuators used in this work. This is 0.13 % of the inviscid flow power (Power $= \rho_\infty U_\infty^3 A_{\text{test-section}}$).

2.2 Flow diagnostics

Qualitative flow characterization was performed using schlieren imaging. Schlieren (as a density gradient based measurement technique) primarily provides data regarding the wave structure. This allows the baseline flow to be observed and confirmed as the desired flow. Additionally, the mean interaction length can be measured. Moreover, any changes in the wave structure due to the LAFPAs can be observed using this fast, easy, low-cost measurement technique. Schlieren also supplies a qualitative metric of the general quality and cleanliness of the flow.

Surface oil flow visualization (SOFV) added qualitative information regarding the interaction shape across the tunnel span. The oil used was a mixture of gear oil, oil paint pigment, and oleic acid (an anti-coagulant). A thin coat of the mixture was applied to the test section floor, and the flow was started quickly. The primary purpose of the SOFV was to supplement the largely centerline measurements used in this study with the full spanwise signature of the interaction region on the test section surface.

Two-component particle image velocimetry (PIV) on a streamwise-vertical plane was the primary data metric for the forced cases. It gives quantitative data regarding the changes in the interaction introduced by the LAFPAs. The PIV data were acquired using the commercially available DaVis 7.2 PIV software and a LaVision Imager Pro-X camera. Seed particles were olive oil with a diameter of approximately 1 micron; they are generated by two TSI 6-jet atomizers in parallel. Illumination was provided by a Spectra Physics Quanta-Ray PIV 400 laser. Cross-correlation and post-processing were performed by DaVis. MATLAB was used to average, organize, and otherwise reduce the data. Multiple runs at a given flow condition were used to collect sufficient data for statistical convergence. This was necessary because oil buildup on the windows obscured the test section before sufficient data could be collected. Using multiple runs for a given case also ensured that the results were repeatable. Further information regarding PIV data collection and processing can be found in Webb (2013).

Time-resolved pressure measurements on the tunnel centerline allowed the SWBLI unsteadiness to be quantitatively examined and compared to literature. The pressure measurements were collected by Kulite XTL-140-25A pressure transducers. The data were acquired at 50 kHz, and an analog hardware low-pass filter was applied with a filter frequency of 25 kHz. The data were taken in de-correlated blocks of 4,096 samples which yields a lowest resolvable frequency of 12.2 Hz. 200 blocks of data were taken for each measurement. Spectra of the data were generated in MATLAB and all weighting, normalizing, etc., were performed in MATLAB.

2.3 Uncertainty analysis

Detailed analysis of uncertainty of experimental data allows random fluctuations to be distinguished from statistically significant trends. Several factors can add uncertainty to PIV data; random error and particle lag were deemed most important in this work. The effect of random error on data uncertainty is well known and easily quantified using conventional statistics. In brief, the variance in the data can be used to calculate a confidence interval that describes the probability that the true mean lies within a certain range of the measured value. Confidence intervals with a confidence level of 95 % (i.e., there is a 95 % chance that the true mean is within the specified interval) were calculated and used to determine the uncertainty in the calculated boundary layer properties (see Table 1).

Additionally, it became important to determine the degree of precision with which shocks could be located. This allowed the statistical significance of the observed shock displacements to be determined. In order to convert the uncertainty in the velocity to uncertainty in shock location, the effect of particle lag must be taken into account. The momentum of the seed particles causes a lag in the particle response to the flow through regions of high velocity gradient, such as shocks. This results in shocks being smeared in the measured velocity maps. The uncertainty in the shock location can be determined by calculating how far the velocity profile of the shock could be shifted and remain within the error bars velocity. The 95 % error bars (calculated as described in the previous paragraph) were used to determine the uncertainty in the shock location, and, by extension, displacement, and this uncertainty has been plotted on the graphs of shock displacement below.

2.4 Experimental approach

The primary purpose of this work is to further improve the understanding of the physics of SWBLIs and to investigate the LAFPAs' ability to control a SWBLI. The hypothesized control mechanism is the potential manipulation of natural instabilities by the introduction of appropriate perturbations. The Kelvin–Helmholtz instability proposed by Pipponiau et al. (2009) is particularly intriguing because of its direct relationship to the size of the separation region. The separation could potentially be mitigated by manipulating the instability. Using this hypothesis as a starting point, the investigation was begun by using the appropriate location for the actuators and forcing frequency. The receptivity region for shear layer instabilities is usually around the shear layer origin. Therefore, the LAFPAs were initially located near the upstream end of the interaction (upstream of the separation line) to allow the perturbations to be convected directly to the hypothesized sensitive region. The most intuitive frequency at which to operate the LAFPAs is that of the measured low Strouhal number unsteadiness, $St = 0.03$.

These forcing parameters were used as an initial investigation step. From there, both actuator location and frequency were varied, and the effect on the SWBLI observed. Additionally, other forcing parameters, such as duty cycle, were varied to determine their effect on the control authority. Based on the response of the flow, further testing with a variety of parameters was conducted in an attempt to better understand the LAFPAs' effects on the flow.

3 Results and discussion

3.1 Baseline characterization

Before examining the LAFPAs' control authority, the baseline flow was characterized. Figure 3 shows a long-exposed (time-averaged) schlieren image. The visible upstream waves are of perturbation strength. This was verified using PIV measurements (see Fig. 7a). The average image allows the interaction length to be determined (as denoted in Fig. 3), defined here as the distance between the (mean) reflected shock foot and the inviscid, primary shock impingement location. This distance was measured to be approximately 39 mm. The interaction length is used as a characteristic length scale in defining the Strouhal number of the unsteady behavior of the interaction region and the forcing frequency. This method of frequency normalization, involving the freestream velocity and the interaction length, has been shown to collapse the unsteadiness frequency from a wide variety of interactions onto a single curve (Dupont et al. 2006). Part of the motivation for expanding the facility was to lengthen the shock generator and move the expansion fan from its trailing edge further downstream. In the preliminary study, the expansion impinged on the trailing edge of the interaction ($X^* = 0$). This imposed a favorable pressure gradient on the boundary layer that would not be present in a real inlet. Enlarging the facility allowed the expansion to be moved downstream to $X^* = 0.54$ ($X/\delta \sim 4$). This significantly reduced the influence of the unrepresentative pressure gradient on the interaction.

Streamwise PIV measurements on the tunnel centerline provided a quantitative view of the interaction. Upstream boundary layer data were also obtained from PIV. The state of the incoming boundary layer, in addition to the shock strength and sidewall boundary layers (corner flows), is crucial to determining the interaction size, shape, severity, unsteadiness, etc. Thus, a characterization of it is essential to fully understand the interaction in which the LAFPAs
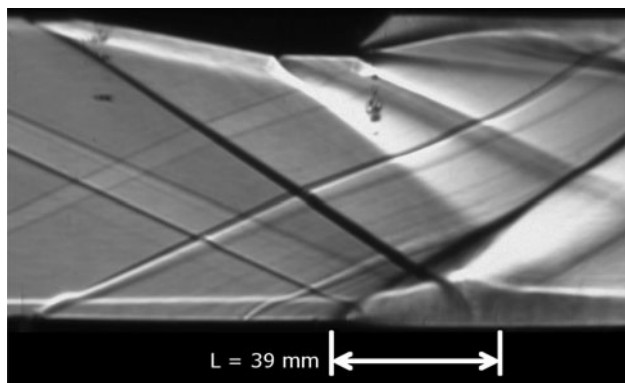
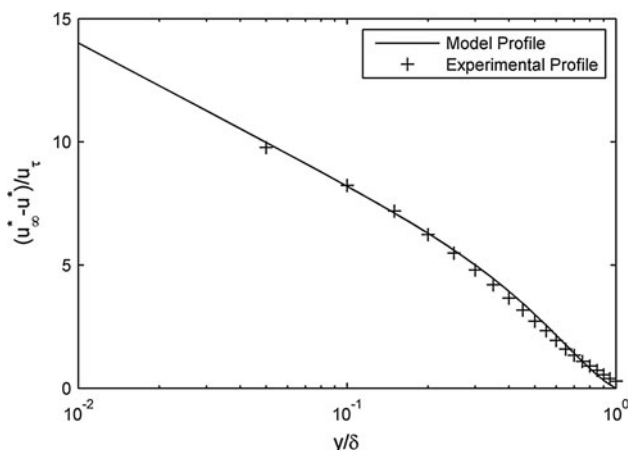**Fig. 3** Baseline average schlieren image

Fig. 4 Velocity profile using van Driest transformation and Maise and McDonald (1968) model profile

are being tested. Table 1 details freestream flow properties and upstream boundary layer properties. The boundary layer thickness (δ) is defined based on a 0.99 U_∞ criterion, and the integral thicknesses are calculated in both an incompressible and a compressible manner for completeness. Incompressible statistics are denoted with a subscript "i." When calculating the compressible values, the density profile was estimated using the technique proposed in Maise and McDonald (1968). The choice of incompressible statistics yields a more widely used metric pp. 21 (Babinsky and Harvey 2011). The Reynolds number based on the boundary layer thickness, and compressible and incompressible momentum thicknesses are also tabulated. The

Reynolds number most commonly referenced in literature is based on the momentum thickness (primarily incompressible).

The boundary layer nature (laminar, transitional, or turbulent) has significant effect on the interaction. Due to the long distance over which the boundary layer developed, it was assumed to be turbulent, and the incompressible shape factor of 1.37 confirmed this assumption. Maise and McDonald developed a model profile for turbulent, compressible, adiabatic boundary layers (Maise and McDonald 1968). This profile uses the van Driest transformation to collapse compressible boundary layers, with a variety of freestream Mach numbers, to a single profile. Equation 1 is the Maise and McDonald profile

$$\frac{u_\infty^* - u^*}{u_\tau} = \frac{1}{\kappa}\ln\left(\frac{y}{\delta}\right) + \frac{\Pi}{\kappa}\left(1 + \cos\left(\frac{\pi y}{\delta}\right)\right) \tag{1}$$

where κ represents the Karmen mixing length constant, Π is the wake strength parameter, and u_τ is the friction velocity. The Maise and McDonald model used $\kappa = 0.4$ and $\Pi = 0.5$. The normalized velocities used in the transformation are defined by Eqs. 2–4.

$$u^* = \frac{u_\infty}{A}\sin^{-1}\left[\frac{2A^2(u/u_\infty) - B}{\sqrt{B^2 + 4A^2}}\right] \tag{2}$$

$$A^2 = \frac{[(\gamma - 1)/2]M_\infty^2}{T_w/T_\infty} \tag{3}$$

$$B = \frac{1 + [(\gamma - 1)/2]M_\infty^2}{T_w/T_\infty} - 1 \tag{4}$$

A comparison of the van Driest transformed upstream boundary layer profile to the model profile is shown in Fig. 4. The observed excellent agreement is another confirmation that the incoming boundary layer is fully turbulent.

Corner flows have been shown to have significant influence on the streamwise size/separation severity of the nominally two-dimensional region of the interaction (Burton and Babinsky 2012; Babinsky et al. 2013). Most of the flow diagnostics used in this study (schlieren, streamwise PIV, time-resolved pressure measurements) record conditions only along the tunnel centerline or integrated across the tunnel span. SOFV provided information regarding the corner flows. A SOFV image is shown in Fig. 5. The shock wave is two-dimensional over 50–60 % of the tunnel span,

Table 1 Upstream boundary layer properties

M_∞	u_∞ (m/s)	δ (mm)	δ_i^* (mm)	θ_i (mm)	H_i	δ^* (mm)	θ (mm)	H
2.33	553 ± 0.06	5.28 ± 0.1	0.82 ± 0.03	0.60 ± 0.01	1.37 ± 0.07	1.57 ± 0.03	0.44 ± 0.02	3.60 ± 0.27

Re (1/m)		Re_δ			Re_θ			$Re_{\theta i}$
36.8×10^6		199,000			16,100			22,000

but the reattachment line highly three-dimensional. This is not surprising as the separated flows are typically three-dimensional. SOFV also clearly verified the presence of separation. None of the other flow metrics used were able to detect the separation due to its small vertical dimension. SOFV revealed an interaction shaped similarly to that of the thin to moderate boundary layer case observed by Baruzzini et al. (Baruzzini et al. 2012).

The influence of the corners on the centerline of oblique impinging SWBLIs is not currently well established. Some postulate that the effect is complex and depends on the relative geometry of the interaction (Babinsky et al. 2013). Regardless of the true influence, the corner flows are qualitatively documented for the benefit of the readers.

As previously mentioned, the centerline time-resolved pressure measurements are of special interest to determine whether the unsteady nature of the interaction region depends on the nature of its generation. Figure 6 shows the unsteadiness data for the compression ramp generated interaction. The weighting and normalization of the PSD curves were carried out as described in Dupont et al. (2006), in particular, the normalized frequency (St_L) is defined as $St_L = f\,L_{int}/U_\infty$. It should be noted that the curves are normalized such that the area beneath each curve is unity; therefore, the amplitude of the fluctuations cannot be compared from one streamwise location to another. The purpose of this plot is to observe how the most energetic frequency changes at different locations within the interaction.

The wedge facility was designed with the intent of minimizing introduced unsteadiness in the interaction. The wedge flow was expected to be cleaner than a compression
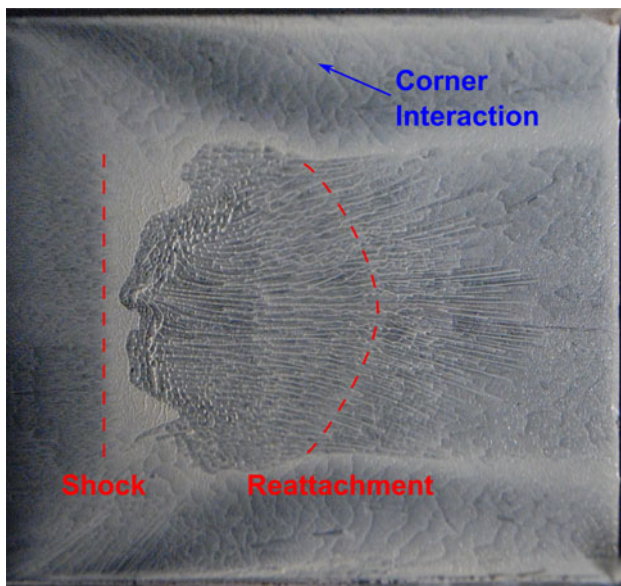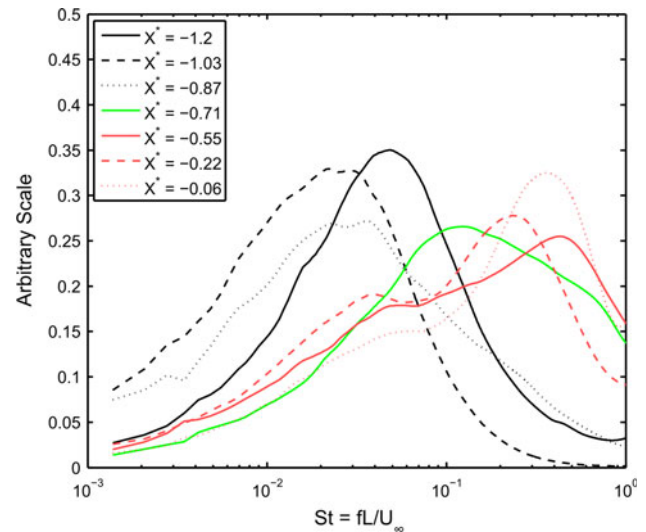
Fig. 6 Weighted and normalized PSD plots of surface pressure within the SWBLI at various streamwise locations

ramp generated SWBLI due to the steady nature of a shock originating in the freestream flow, rather than in the ceiling boundary layer. However, comparing these results to the previous work (Webb et al. 2011), the observed unsteadiness appears to be quite similar for the wedge and ramp generated SWBLIs. The salient features observed in literature, (1) peak energy content around $St = 0.03$ in the reflected shock impingement region, and (2) peak energy content around $St = 0.5$ in the downstream regions of the interaction, are present in both cases. The only notable difference between this and the previous work is that here the transition to higher frequencies appears to take place further downstream within the interaction. However, this location is more consistent with literature (Touber and Sandham 2009; Dupont et al. 2006).

The time-resolved pressure measurements were also performed to determine initial actuation parameters. As previously mentioned, the starting assumption for this investigation is that the LAFPAs would provide perturbations necessary to excite the shear layer instabilities in order to control the interaction process. The shear layer vortex shedding has been suggested to be the source of the low-frequency unsteadiness of the reflected shock (Piponniau et al. 2009). Thus, the pressure data from this region are a direct measure of the peak frequency of this unsteadiness and potential instability. This provided a starting point in the forcing parameter space.

3.2 LAFPA control authority

In order to test the LAFPAs' effectiveness, according to the previously determined initial parameters, the LAFPAs were placed at a streamwise location of $X_a^* = -0.83$ (see Fig. 2) and operated in-phase at $St_F = 0.03$. PIV data

Fig. 5 Surface oil flow visualization image

provided the primary quantitative measure of the effects of the LAFPAs. Figure 7 compares the streamwise and vertical velocity fields of baseline and forced flows.

In order to accentuate the differences caused by the actuators, the velocity fields of the baseline were subtracted from those of the forced case. The fields of velocity difference are shown in Fig. 8. The observed differences were determined to be statistically significant with 95 % confidence. The immediately obvious effect of the actuators is to move the reflected shock upstream of its baseline location. This is clearly seen in the slanted dark line through the vertical velocity difference field. The upstream edge of the line corresponds to the reflected shock location in the forced case, and the downstream edge to its location in the baseline case. A careful examination of Fig. 8 also shows that the interaction region seems to move slightly upstream. Other than a positional shift, the velocity fields for the forced case are nearly identical to those of the baseline. In particular, the interaction region has not been reduced, rather it has been enlarged (see Fig. 7).

While the apparent shift of the interaction upstream shows the significant effect of the LAFPAs on the SWBLI, it is not clear how such a modification is a useful control objective. Phase-locked PIV measurements were therefore used to gain further insight into what was occurring. The PIV software provides the capability to trigger image acquisition using an external, cyclic trigger signal. This feature was used to synchronize the image acquisition to the trigger signal sent to the LAFPA power supply. Thus, the PIV acquisition was locked to a particular phase in the LAFPA forcing period, for example, 0°—just begun arcing, 180°—just stopped arcing (for 50 % duty cycle). This allowed the collection of data that showed what the interaction looked like, on a phase-averaged basis, at different points throughout the forcing period. Figure 9 shows the results of an equally distributed eight-phase sweep at the initial forcing conditions. In order to facilitate easy comparison of the eight velocity difference fields, the shock displacement at each phase was measured from the velocity difference fields and plotted. The LAFPAs have just begun arcing at phase 1 and just stopped arcing at phase 5. The reflected shock begins to move upstream as soon as the LAFPAs begin arcing and continues to do so until the actuators stop arcing. The shock then begins to relax back toward its baseline location. This frequency, however, does not appear to allow sufficient time for the shock to relax completely before the next forcing period begins. This effect is similar to that observed by Narayanswamy et al. (2012). The postulated mechanism in that work was that the reduced Mach number in the boundary layer, due to the heating generated by the actuators, allowed the shock to propagate upstream.

Fig. 7 Streamwise PIV velocity fields, **a** baseline flow, **b** forced flow
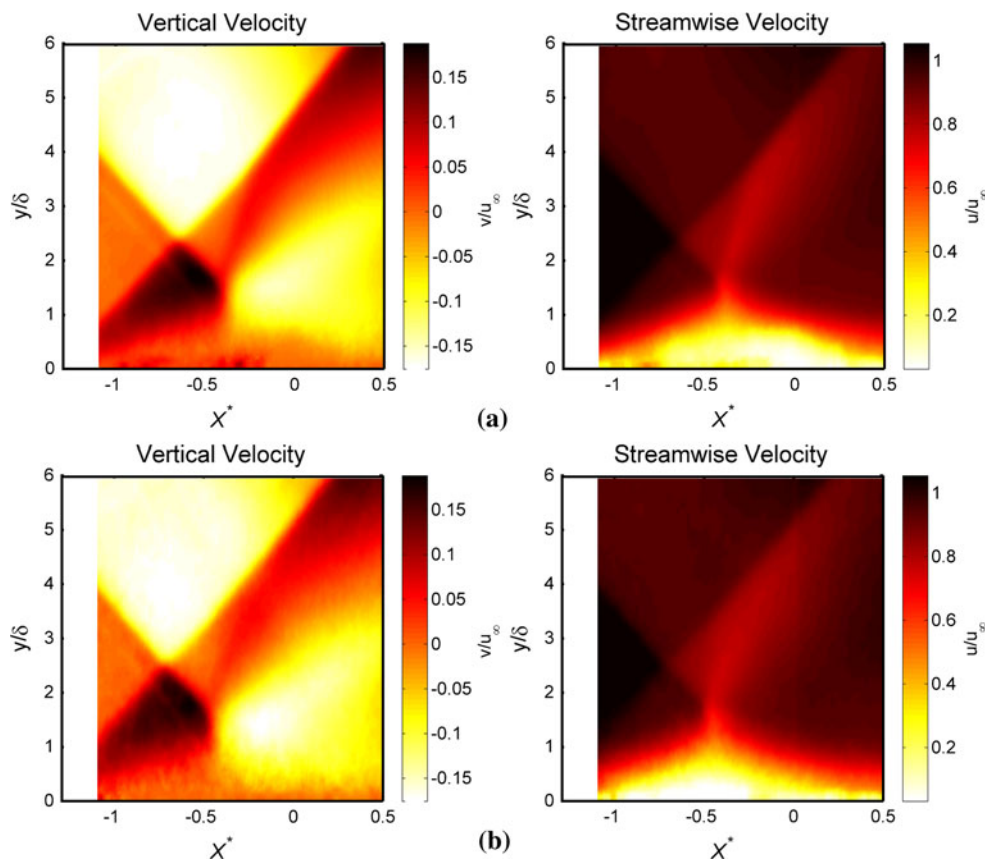
Fig. 8 Ensemble-averaged velocity difference fields with forcing Strouhal number $St_F = 0.03$
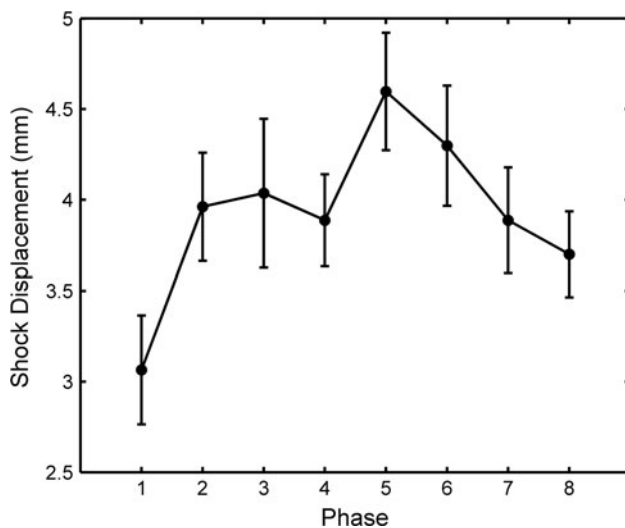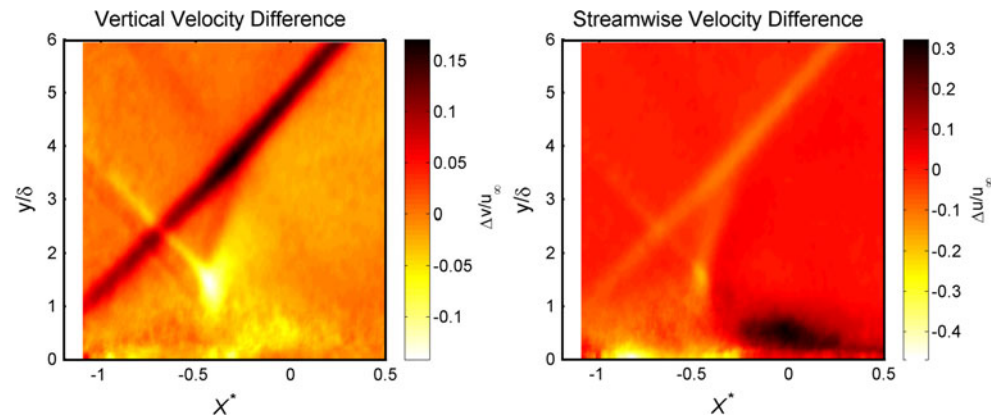

Fig. 9 Shock displacement at a variety of phases with $St_F = 0.03$ and DC = 50 %

Fig. 10 Schlieren image showing the various streamwise locations used for the LAFPAs

It was not clear from the above results whether the LAFPAs were exciting an instability, or whether the observed effects were merely due to a modification of the upstream boundary layer. When exciting an instability, the location of actuation is critical, and the effect is maximized when actuation is at the maximum receptivity location. Thus, it was decided to vary the LAFPAs' location to investigate whether the LAFPAs were simply not close to the receptivity location, which is expected to be just upstream of the separation location in this case. Still operating under the assumption that the sensitive region would be in the vicinity of the separation line (shear layer origin), the LAFPAs' streamwise location was varied from $X_a^* = -1.09$ to $X_a^* = -0.77$ (see Fig. 10). Surprisingly, almost no difference in the LAFPAs' effectiveness was observed for the locations tested. Although not statistically significant, a slightly larger effect was observed when the LAFPAs were located at $X_a^* = -0.96$; thus, the rest of the experiments were performed with the LAFPAs in this location (see Fig. 10).
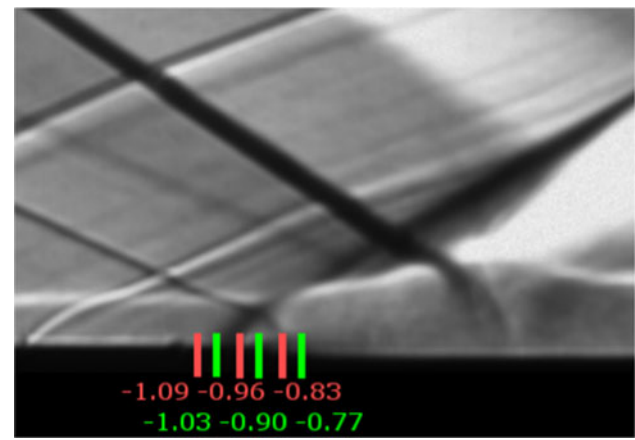
The frequency dependence of the control authority was also investigated. The frequency of the actuators was varied from $St_F = 0.0075$ to $St_F = 1.5$. Figure 11 shows the shock displacements for two phases: the phases of "maximum displacement" and "maximum relaxation" (corresponding to minimum displacement). Many of the test cases have statistically identical shock displacements; but it is clear that the overall trend (in both phases) is that increasing the frequency increases the shock displacement. At some frequency, there appears to be a saturation of this effect, and the shock displacement no longer changes significantly as the frequency is increased. Higher frequencies have shorter periods, which mean there is less time for the reflected shock to relax between LAFPA pulses. This explains the behavior of the maximum relaxation. The maximum displacement trend follows a similar idea: the reflected shock is moved upstream by the actuators, and due to the smaller relaxation time at high frequencies, the maximum relaxation point is further upstream, thus resulting in a greater maximum displacement. Although this reasoning makes sense, the trend is slightly confusing given the significantly longer arcing time present at the
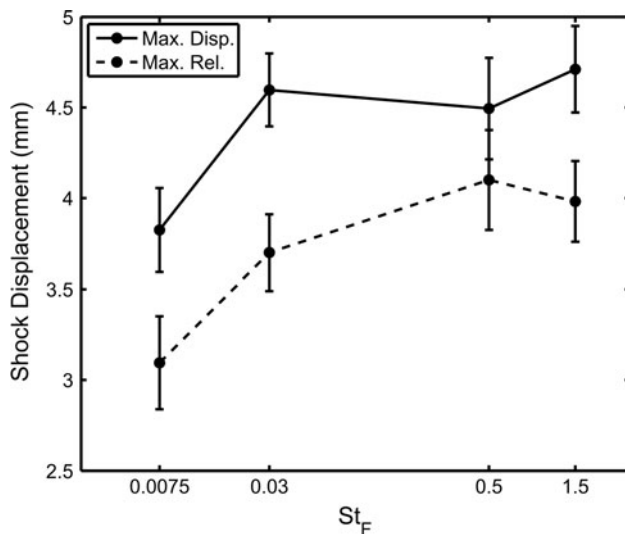
Fig. 11 Shock displacement at a variety of forcing Strouhal numbers

Fig. 12 Shock displacement at a variety of duty cycles

lower frequencies. This may be indicative of some sort of saturation occurring when forcing at low frequencies.

It was also of interest to explore how the duty cycle of the LAFPAs affected their control authority. The actuators were operated at duty cycles of 10, 30, and 50 %. The shock displacements, measured from the velocity fields corresponding to the maximum displacement and relaxation, are shown in Fig. 12. This study was performed for an actuator frequency of $St_F = 0.03$. An inspection of the results clearly shows that a higher duty cycle results in greater displacement. This seems intuitive given what was found in the frequency sweep. Namely, a longer duty cycle results in more time spent arcing; therefore, the overall shock displacement is greater because it does not relax as far. Moreover, each time the LAFPAs begin arcing the reflected shock position is further upstream due to the smaller relaxation time. Furthermore, a longer arcing time may allow the displacement to saturate rather than stopping actuation when the reflected shock has only moved upstream partway. This can be seen by the maximum displacement of the shock for the 30 and the 50 % cases.

3.3 Discussion of flow control mechanism

The starting hypothesis of this work was that the actuators would manipulate the low-frequency unsteadiness in the upstream portion of the interaction region, believed to be associated with the shear layer instability over the separated region, to generate large changes with minimal power input. This type of excitation has proven effective in subsonic and supersonic cold and hot jets (Samimy et al. 2007, 2012), cavity flows (Yugulis et al. 2013), and using a different kind of plasma actuator with a similar control mechanism in flow over an airfoil (Little et al. 2012;
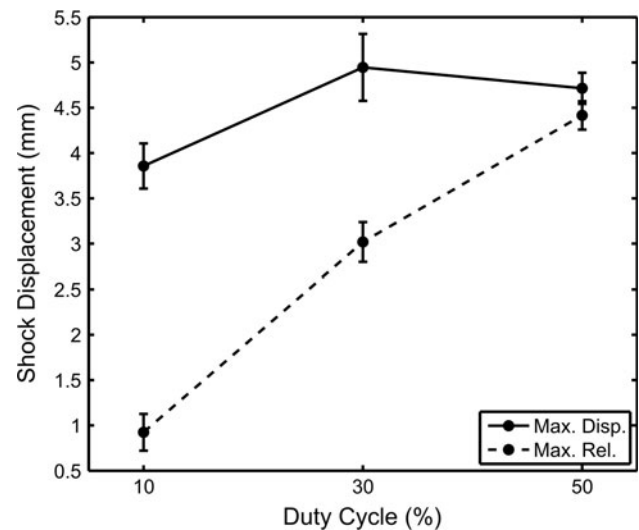
Rethmel et al. 2011). However, the results (see LAFPA control authority) do not appear to support this hypothesis in the current work. It should be noted that flows such as jets and cavities have well known and researched instabilities. However, SWBLI possesses unsteadiness (Fig. 6) but there is not yet an established instability associated with this unsteadiness.

When manipulating a natural instability, there is normally a set or range of frequencies at which perturbations produce significant effects, and a forcing frequency at which the effectiveness is maximized. This study sought to manipulate the low-frequency unsteadiness associated with the upstream region of the interaction, assuming that the unsteadiness is associated with an instability. Using that hypothesis as the focus of the research did not identify a "peak-effectiveness" frequency, rather it appears that increasing the frequency increases the effectiveness within the investigated range ($St_F \leq 1.5$). It could be argued that no peak was discovered because the highest tested frequency was not sufficiently high. If this is the case, however, it is not immediately apparent what the natural manifestation of the forced instability is. It is known and shown above (Fig. 6) that there are natural oscillations within the interaction between $St = 0.03$ and 0.5; however, apart from the upstream boundary layer turbulence ($St \sim 7$), there are no other notable oscillations of frequency higher than the highest tested forcing frequency: $St_F = 1.5$. Thus, it seems likely that no peak-effectiveness frequency was discovered because one does not exist (for the LAFPAs located upstream of the SWBLI).

Varying the LAFPAs' streamwise location also yielded interesting results. Namely, within the tested region, there was little or no variation in the LAFPAs' effectiveness. This lack of sensitivity to actuation location was another

indication that either there is no instability associated with the observed low-frequency unsteadiness or it simply does not render itself to excitation.

These two results seem to indicate clearly that the shock displacement induced by the LAFPAs is not due to the postulated low-frequency instability manipulation. If this is the case, then what is the LAFPAs' control mechanism? Work by Jaunet et al. (2012) has shown that heating the boundary layer moves the reflected shock upstream. They suggest that this is a result of the change in density introduced by the heating. The density changes affect the mass balance within the separation bubble resulting in a spatially expanded bubble (Souverein et al. 2013). This effect is similar to what has been observed in this work, although the magnitude of the effect in this work is significantly smaller. The idea of heating being the control mechanism seems to fit well with the lack of dependence on control location (as long as the LAFPAs are upstream of the separation) and the observed dependence on frequency, that is, given less time for the flow to relax after actuation (heat addition), the displacement is greater. This also makes sense given the observed increasing displacement with increasing duty cycle (increased time-averaged power addition). However, the heating/energy imparted to the flow by LAFPAs is estimated to be nearly two orders of magnitude less than that used by Jaunet et al. (2012) This difference could be due to the energy density of the actuators compared to a heated wall and/or the higher instantaneous rate of energy deposition of the LAFPAs.

The effects seem rather large given the small amount of energy the LAFPAs are actually introducing to the flow. Therefore, although the observed trends in control authority seem to point to a heating mechanism, a more thorough investigation was conducted. Heating affects the interaction by degrading the boundary layer health, making it less resistant to separation, thereby lengthening the interaction. Souverein addresses the topic of proper interaction length scaling (Souverein et al. 2013). For the case addressed in this work, namely when the strength of the impinging shock remains constant, the length of the interaction should be directly proportional to the boundary layer displacement thickness. It should be noted that nothing in the scaling work indicates that the expansion of the interaction would be in the upstream direction; but this is a natural assumption because the location of the downstream end of the interaction is determined by the free-stream conditions.

As previously stated, the maximum interaction length increase was approximately 5 mm and the interaction length was measured to be 39 mm. Averaging over the phases shows that the mean shock displacement was approximately 4 mm. Thus, the interaction length was increased by about 10 %, on the mean, and for a heating

mechanism to be viable, the LAFPAs must be capable of increasing the incoming boundary layer displacement thickness by the same relative amount. An estimate of the boundary layer thickness increase by the LAFPAs was undertaken. Quasi-one-dimensional, adiabatic, perfect gas flow was assumed. The wall-normal pressure gradient was also assumed to be zero. The entire power input was assumed to affect the flow solely by modifying the total temperature (and thereby the density), that is, strictly by Joule heating. The downstream total temperature profile shape was estimated using a basic knowledge of heat transfer and scaled to model the experimental power input. With these assumptions, the downstream density profile can be calculated (see Eq. 5, derived from the ideal gas law).

$$\rho(y)/\rho_\infty = \frac{T_\infty}{T_o(y) - \frac{\gamma-1}{2\gamma R}u^2(y)} \tag{5}$$

Although the LAFPAs have been assumed to affect the flow only through Joule heating, they will still have an indirect effect on the velocity profile. This will primarily be through the altered skin-friction coefficient and the adjustment in the boundary layer equilibrium that will result. To account for this effect, an experiment was conducted in which the LAFPAs forced the undisturbed boundary layer (without the shock generator in the tunnel). Centerline, streamwise, two-component PIV data were collected for the actuators forcing at two frequencies: $f = 1$ kHz and 20 kHz. The duty cycle for both cases was 50 %. The downstream baseline and forced profiles were used appropriately in the above analysis. It should be noted that due to the corruption from the LAFPAs, PIV data could not be taken in their vicinity. Therefore, the baseline and forced profiles used in the calculation were scaled to match the displacement thickness at the LAFPAs' location. There was some question as to whether the displacement thickness or boundary layer thickness is the correct normalization in this case. Both were examined, and the results were only slightly altered: the conclusions are the same. Thus, it was decided to use the displacement thickness normalization. It was found that the necessary temperature profile required 0.40 kW for the 1 kHz case and approximately 0.38 kW for the 20 kHz case to generate the observed elongation of the separated region. With the experiment accounting for all mechanisms (known and unknown) of the LAFPAs, it seems that the LAFPAs are able to generate the necessary displacement thickness increase in the upstream boundary layer to cause the observed length increase in the SWBLI.

Thus, the LAFPAs' control authority does not appear to depend on the presence of the SWBLI, rather the control is introduced through the interaction between the LAFPAs and the upstream boundary layer. This clearly indicates

that the LAFPAs are not controlling the interaction through instability manipulation in this configuration. This does not preclude the possibility that the LAFPAs could manipulate instabilities in the SWBLI to control it in other configurations, such as near the reattachment line of the separation region. This will be investigated in the future.

4 Conclusions

The control authority of the LAFPAs was investigated in a Mach 2.3, impinging, SWBLI with a turbulent boundary layer of $Re_{\theta i} = 22,000$. The baseline flow was characterized and found to be in good agreement with the literature. Power spectra along the centerline of the baseline flow with the compression ramp generated impinging shock were similar in nature to those previously documented in the wedge-generated interaction.

The primary observed effect of the LAFPAs' forcing was to move the reflected shock upstream by approximately one boundary layer thickness (~ 5 mm). Phase-locked PIV data were used to document more accurately the interaction's response to the LAFPAs. This showed that the displacement was largest during the part of the forcing period that the LAFPAs were arcing. Parametric sweeps determined that the LAFPAs' control authority did not depend on their streamwise location, within the range explored, and increased with increasing frequency and duty cycle. These trends do not support the hypothesis that the LAFPAs' control mechanism is a manipulation of the low-frequency unsteadiness in the upstream part of the interaction. If, however, the LAFPAs are merely heating the flow, this behavior and trend make much more sense.

Upon further investigation of the LAFPAs' effects, it was found that the LAFPAs are capable of sufficiently increasing the boundary layer displacement thickness to generate the observed expansion of the interaction, even in an undisturbed boundary layer. Thus, it is concluded that the LAFPAs' control mechanism in this configuration is not instability manipulation, but a modification of the incoming boundary layer. This modification is thought to take place primarily through heat addition and associated mechanisms.

References

Anderson B, Tinapple J, Surber L (2006) Optimal control of shock wave turbulent boundary layer interactions using micro-array actuation, 3rd AIAA Flow Control Conference p 3197

Andreopoulos J, Muck K (1987) Some new aspects of the shock-wave/boundary-layer interaction in compression-ramp flows. J Fluid Mech 180:405–428

Babinsky H, Harvey J (2011) Shock wave-boundary-layer interactions. Cambridge University Press, New York

Babinsky H, Ogawa H (2008) SBLI control for wings and inlets. Shock Waves 18(2):89–96

Babinsky H, Li Y, Ford C (2009) Microramp control of supersonic oblique shock-wave/boundary-layer interactions. AIAA J 47(3):668–675

Babinsky H, Oorebeek J, Cottingham T (2013) Corner effects in reflecting oblique shock-wave/boundary-layer interactions, 51st AIAA Aerospace Sciences Meeting p 0859

Baruzzini D (2012) An industry perspective on the role of bleed in high-speed inlet design process, Private Communication

Baruzzini D, Domel N, Miller D (2012) Addressing corner interactions generated by oblique shock-waves in unswept right-angle corners and implications for high-speed inlets, 50th AIAA Aerospace Sciences Meeting: AIAA p 0275

Beresh S, Henfling J, Spillers R, Pruett B (2011) Very-large-scale coherent structures in the wall pressure field beneath a supersonic turbulent boundary layer, 49th AIAA Aerospace Sciences Meeting, p 746

Burton D, Babinsky H (2012) Corner separation effects for normal shock wave/turbulent boundary layer interactions in rectangular channels. J Fluid Mech 707:287–306

Caraballo E, Webb N, Little J, Kim J-H, Samimy M (2009) Supersonic inlet flow control using plasma actuators, 47th AIAA Aerospace Sciences Meeting p 924

Dolling D (2001) Fifty years of shock-wave/boundary-layer interaction research: what next? AIAA J 39(8):1517–1531

Dolling D, Brusniak L (1989) Separation shock motion in fin, cylinder, and compression ramp-induced turbulent interactions. AIAA J 27(6):734–742

Dupont P, Haddad C, Debiève J-F (2006) Space and time organization in a shock-induced separated boundary layer. J Fluid Mech 559:255–277

Ganapathisubramani B, Clemens N, Dolling D (2009) Low-frequency dynamics of shock-induced separation in a compression ramp interaction. J Fluid Mech 636:397–425

Gefroh D, Loth E, Dutton C, McIlwain S (2002) Control of an oblique shock/boundary-layer interaction with aeroelastic mesoflaps. AIAA J 40(12):2456–2466

Hahn C, Kearney-Fischer M, Samimy M (2011) On factors influencing arc filament plasma actuator performance in control of high speed jets. Exp Fluids 37:5

Jaunet V, Debiève J-F, Dupont P (2012) Experimental investigation of an oblique shock reflection with separation over a heated wall, 50th AIAA Aerospace Sciences Meeting AIAA p 1095

Kalra C, Zaidi S, Miles R, Macheret S (2011) Shockwave-turbulent boundary layer interaction control using magnetically driven surface discharges. Exp Fluids 50:547–559

Lee S, Goettke M, Loth E, Tinapple J, Benek J (2010a) Microramps upstream of an oblique-shock/boundary-layer interaction. AIAA J 48(1):104–118

Lee S, Loth E, Babinsky H (2010) Normal shock boundary layer control with various vortex generator geometries, AIAA 5th Flow Control Conference p 4254

Little J, Takashima K, Nishihara M, Adamovich I, Samimy M (2012) Separation control with nanosecond-pulse-driven dielectric barrier discharge plasma actuators. AIAA J 50(2):350–365

Maise G, McDonald H (1968) Mixing length and kinematic eddy viscosity in a compressible boundary layer. AIAA J 6(1):73–80

Narayanaswamy V (2010) Investigation of a pulsed-plasma jet for separation shock/boundary layer interaction control. Dissertation, University of Texas at Austin

Narayanaswamy V, Raja L, Clemens N (2012) Control of a shock/boundary layer interaction by using a pulsed-plasma jet actuator. AIAA J 50(1):246–249

Piponniau S, Dussauge J, Debieve J, Dupont P (2009) A simple model for low-frequency unsteadiness in shock-induced separation. J Fluid Mech 629:87–108

Pirozzoli S, Grasso F (2006) Direct numerical simulation of impinging shock wave/turbulent boundary layer interaction at M = 2.25. Phys Fluids A 18:1–17

Rethmel C, Little J, Takashima K, Sinha A, Adamovich I, Samimy M (2011) Flow separation control using nanosecond pulse driven DBD plasma actuators. Int J Flow Control 3(4):213–232

Samimy M, Kim J-H, Kastner J, Adamovich I, Utkin Y (2007a) Active control of high-speed and high-Reynolds-number jets using plasma actuators. J Fluid Mech 578(1):305–330

Samimy M, Kim J-H, Kastner J, Adamovich I, Utkin Y (2007b) Active control of a mach 0.9 jet for noise mitigation using plasma actuators. AIAA J 45(4):890–901

Samimy M, Kim J-H, Kearney-Fischer M, Sinha A (2010) Acoustic and flow fields of an excited high Reynolds number axisymmetric supersonic jet. J Fluid Mech 656:507–529

Samimy M, Kearney-Fischer M, Kim J-H, Sinha A (2012) High-speed and high-Reynolds-number jet control using localized arc filament plasma actuators. J Propul Power 28:2

Shahneh A, Motallebi F (2009) Effect of submerged vortex generators on shock-induced separation in transonic flow. J Aircraft 46(3):856–863

Sinha A, Kim K, Kim J-H, Serrani A, Samimy M (2010) Extremizing feedback control of a high-speed and high Reynolds number jet. AIAA J 48(2):387–399

Solomon J, Kumar R, Alvi F (2010) High-bandwidth pulsed microactuators for high-speed flow control. AIAA J 48(10):2386–2396

Souverein L, Debiève J-F (2010) Effect of air jet vortex generators on a shock wave boundary layer interaction. Exp Fluids 49:1053–1064

Souverein L, Bakker P, Dupont P (2013) A scaling analysis for turbulent shock-wave/boundary-layer interactions. J Fluid Mech 714:505–535

Syberg J, Koncsek J (1976) Experimental evaluation of an analytically derived bleed system for a supersonic inlet. J Aircraft 13(10):792–797

Titchener N, Babinsky H, Loth E (2012) Can fundamental shock-wave/boundary-layer interaction research be relevant to inlet aerodynamics?, 50th AIAA Aerospace Sciences Meeting, AIAA p 0017

Touber E, Sandham N (2009) Large-eddy simulation of low-frequency unsteadiness in a turbulent shock-induced separation bubble. Theoret Comput Fluid Dyn 23:79–107

Touber E, Sandham N (2011) Low-order stochastic modelling of low-frequency motions in reflected shock-wave/boundary-layer interactions. J Fluid Mech 671:417–465

Utkin Y, Keshav S, Kim J-H, Kastner J, Adamovich I, Samimy M (2007) Development and use of localized arc filament plasma actuators for high-speed flow control. J Phys D Appl Phys 40(3):685–694

Webb N (2013) Control of a shock wave-boundary layer interaction using localized arc filament plasma actuators, Dissertation. The Ohio State University

Webb N, Clifford C, Samimy M (2011) Preliminary results on shock wave/boundary layer interaction control using localized arc filament plasma actuators, 41st AIAA Fluid Dynamics Conference p 3426

Yugulis K, Gregory J, Samimy M (2013) Control of high subsonic cavity flow using plasma actuators, 51st AIAA Aerospace Sciences Meeting p 0679